1.A Effects of Illumination Nonuniformities on Direct-Drive ICF Implosions

As an introduction of the effects of illumination nonuniformity on pellet performance, we present results from a direct-drive pellet implosion. Next, the potential role that illumination nonuniformities will play in direct-drive pellet implosions is identified. We have divided the discussion into two broad categories: (1) long-wavelength illumination nonuniformities (those wavelengths for which potential Rayleigh-Taylor unstable growth during the implosion would be small); and (2) short-wavelength nonuniformities (wavelengths for which the potential for exponential growth development during the acceleration phase of the implosion exists). The discussion will show that, although ICF targets are relatively insensitive to isolated long-wavelength (Legendre modes <4) nonuniformities, it is the combination of all modes and their potential mode-mode interactions that must be considered to ensure the success of ICF implosions.

Direct-Drive Pellet Implosion

For this discussion we use a pellet design similar to those used in the recent OMEGA high-density cryogenic implosion experiments.[4] While not all of the conditions required for a low-adiabat, nearly isentropic compression (required for high-gain pellet designs) are met with this target, it is still susceptible to drive distortions and fluid instabilities important to future high-gain designs and, as such, represents an important step in our understanding of future implosions. The pellet, shown schematically in Fig. 37.1, is composed of a 5-μm-thick glass shell with a 125-μm inner radius. The glass shell surrounds a levitated, ~ 4.10-μm-thick cryogenic DT fuel layer (100 atm at room temperature), which in turn surrounds an inner gaseous region of D and T whose density and composition is given by the temperature at which the cryogenic fuel layer is maintained. This type of pellet design is referred to as a "single-shell" design and is similar in nature to future high-gain, direct-drive designs; the main difference being the replacing of the glass ablator with a low-atomic-number (Z) material, such as LiD, CH, or Be.[5] (Due to present target fabrication limitations, experiments have been limited to glass ablators only. The use of low-Z ablators in the cryogenic environment of OMEGA is an area of active research at this time.) The pulse shape used for this simulation was a 650-ps (FWHM) Gaussian with peak power at ~ 1.02 ns from the start of the simulation and 1500 J in the UV (351 nm). The laser-beam spatial profile used was an azimuthally averaged, distributed-phase-plate (DPP) profile.[6] The simulation was performed with the one-dimensional (1-D) hydrodynamics program LILAC.

The processes associated with the implosion of this pellet can be outlined as follows. Initially the laser pulse is incident on the outer surface of the glass ablator. The outer layers of the pellet begin to heat, melt, ionize, and ablate from the pellet surface resulting in an
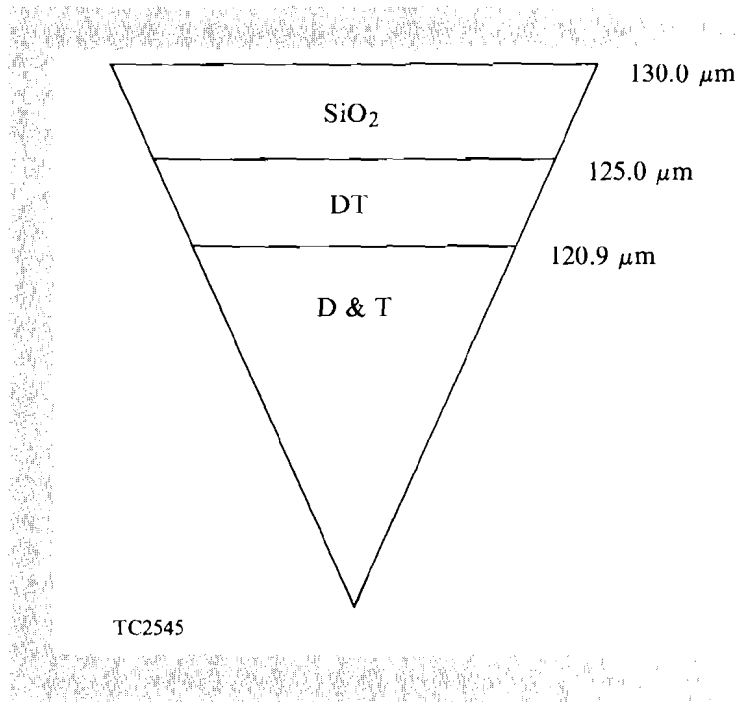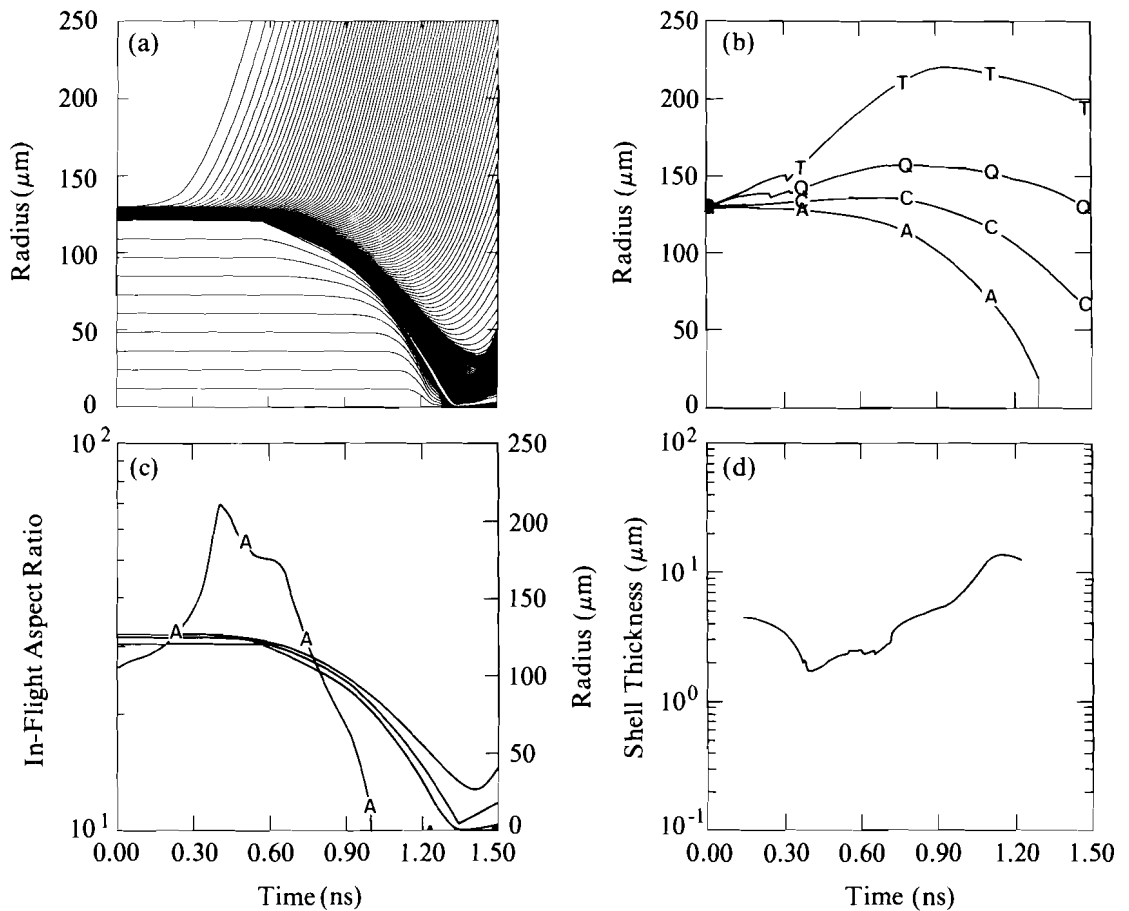
Fig. 37.1
Schematic of single-shell, glass-ablator, OMEGA cryogenic pellet.

outward-expanding, low-density, high-temperature coronal region and an inward-propagating shock wave. The laser energy continues to be deposited, predominantly by inverse bremsstrahlung, in the underdense coronal region. As the laser energy is deposited, energy is transported from the region of deposition (near the critical density region for this implosion) to the unablated pellet material (ablation surface) via electron thermal conduction and, to a lesser extent, ion thermal conduction and radiation transport (x rays generated in the less dense coronal region). This radially inward-conducted energy continues to cause material to ablate from the pellet surface, which results in driving the remaining unablated material inward, acting like a spherical rocket. Figure 37.2(a) displays the radius-versus-time plot for this implosion. The lines in Fig. 37.2(a) represent the motion of Lagrangian fluid markers used in the simulation as a function of time. Those lines that increase in radius as a function of time represent ablated material, while those that decrease represent imploded material. Figure 37.2(b) displays the radius-versus-time history of particular surfaces of interest during the implosion. Figure 37.2(c) displays the in-flight aspect ratio versus time and Fig. 37.2(d) the overdense shell thickness $\Delta R(t)$ as a function of time. [The in-flight aspect ratio $A(t)$ is defined as the time-dependent radius of the overdense shell material $R(t)$ divided by its thickness [i.e., $A(t) = R(t)/\Delta R(t)$]. The shell thickness is determined by locating the peak density in the unablated imploding pellet and then finding the $1/e$ density locations radially outward and inward from this peak density location.[7] The separation of the $1/e$ points determines $\Delta R(t)$ and their average determines $R(t)$. The in-flight aspect ratio and shell thickness are a measure of the susceptibility of a pellet design to unstable hydrodynamic growth development during the implosion. Further discussion appears later in this article.]

3

Fig. 37.2
One-dimensional (*LILAC*) hydrodynamics simulation of implosion of the single-shell OMEGA cryogenic target shown in Fig. 37.1.
(a) Radii-versus-time history.
(b) Radius-versus-time history for: A-ablation surface, C-critical surface, Q-quarter-critical surface, and T-tenth-critical surface.
(c) In-flight aspect ratio (curve labeled A) and layer-interface radii versus time.
(d) Overdense shell thickness versus time.

The stagnation phase of this implosion begins to occur at ~ 1.20 ns. The imploding shell of DT fuel and remaining unablated ablator material are moving inward at $\sim 2.50 \times 10^7$ cm/s at this time. The conversion of shock and kinetic energy and pressure-volume work associated with the continued shell convergence goes into increasing the internal energy of the inner DT-fuel region. The resulting rise in DT-fuel pressure eventually brings the inward motion of the imploding material to a halt at a time referred to as a peak compression. After this time, as shown by the increasing radius trajectories in Fig. 37.2(a) at ~ 1.40 ns, the pellet begins to disassemble. The minimum radius of the fuel-ablator interface for this example was ~ 5.50 μm. This represents a radial convergence ratio (C_R), defined as the initial fuel-ablator interface radius divided by its minimum radius during the implosion, of ~ 25 (high-gain, direct-drive pellet designs have hot-spot convergence ratios of ~ 25). The peak final core conditions obtained from this simulation were mass-averaged fuel density (ρ) of ~ 1300

XLD; mass-averaged ion temperature (T_i) of ~ 0.50 keV; neutron-averaged ion temperature $<T_i>_n$ of ~ 1.90 keV; neutron-averaged fuel areal density (ρR) of ~ 98 mg/cm^2; and neutron-averaged ablator areal density $(\rho \Delta R)$ of ~ 59 mg/cm^2.

As shown in the above discussion, the efficiency of conversion of the shock and kinetic energy to internal energy of the central fuel region and the need for large radial convergence to obtain high final fuel densities are critical for successful ICF implosions, whether driven directly or indirectly, and serve to place strict constraints on the drive nonuniformity that a pellet can tolerate during the implosion. There are two important classes of distortions that can be caused by illumination nonuniformities. The first, commonly referred to as secular distortions, can grow linearly in time (t) and/or as t^2. The second, similar to the classical Rayleigh-Taylor fluid instability at an interface of two inviscid fluids,[8-10] can potentially result in the exponential growth in time of initial distortions.

During the inward acceleration phase of an ICF pellet implosion, the cold, dense shell material is being accelerated by the hot, less-dense ablated material. This situation is analogous to the classical Rayleigh-Taylor fluid instability. Numerical simulations have shown that ablation processes act to modify the linear growth rates and nonlinear mode development from those expected from classical fluid simulations.[11-13] This instability is often referred to as the acceleration phase or outside surface instability. The distinction here is made because, during the stagnation phase of the implosion, the dense imploding shell material is decelerated by the hot, less-dense fuel region. Again this situation closely resembles the classical Rayleigh-Taylor instability at an interface for which the Atwood number[10] $\{[(\rho_h - \rho_l)/(\rho_h + \rho_l)]$, where ρ_h is the density of the dense or heavy fluid and ρ_l is the density of the light fluid} is less than 1 or where the linear growth is modified by the presence of a density scale length.[10,14] This phase of potentially unstable growth development is referred to as the deceleration phase or inside surface instability.
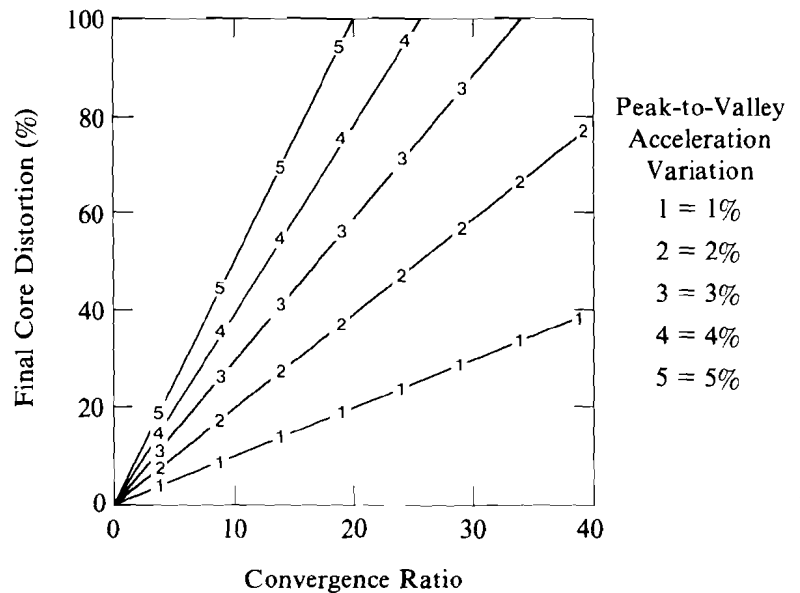
Long-Wavelength Illumination Nonuniformities

For direct-drive laser fusion, long-wavelength illumination nonuniformities can arise from a number of different sources.[15] The dominate sources are (1) the number and placement of individual beams about the target; (2) individual beam mispointing and/or misfocusing; (3) energy balance between individual beams; and, (4) pulse-shape differences between individual beams. Simulations of the contributions to illumination nonuniformity due to the first two sources show that these effects lead to long-wavelength nonuniformities that can change in amplitude during the implosion [due to the motion of the critical surface and coronal plasma formation during the implosion, see Fig. 37.2(b)].[16,17] However, most often they do not result in changes in the phase of the nonuniformities during the implosion. For frequency-tripled glass laser systems, items (3) and (4) have been found to be closely coupled. Energy differences between individual IR (1054-nm) beams can result in not only energy differences in the frequency-tripled UV beams but beam-to-beam pulse-shape variations

due to the nonlinear crystal conversion processes.[18,19] This combined effect of different IR beam energy and the conversion from IR to UV can potentially lead to large-amplitude, long-wavelength modes that can change both in amplitude and phase during the implosion. (The combined effects of items (3) and (4) are referred to as power balance.)

Growth of Rayleigh-Taylor long-wavelength modes should be small. Therefore, constraints on the magnitude of a long-wavelength perturbation that a pellet can tolerate can be obtained from simple dynamics arguments. It can be shown that for secular distortions growing as t^2, the final core distortion δ_F is given by

$$\delta_F = (C_R - 1) \, \Delta a / \bar{a},$$

where C_R is the radial convergence ratio, Δa is the angular variation in the radial acceleration, and $\bar{a}$ is the average radial acceleration. Figure 37.3 displays the calculated-core distortions versus radial-convergence ratio for a number of peak-to-valley acceleration varieties.
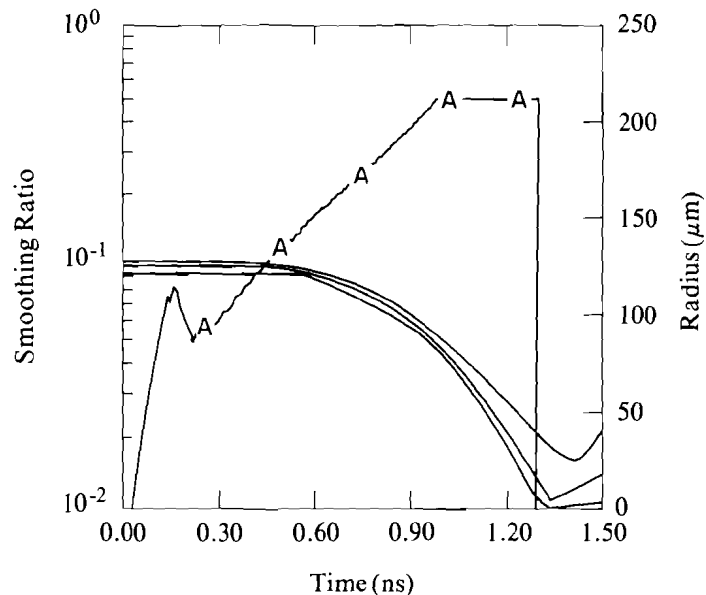

TC2547

Fig. 37.3
Final core distortions versus radial convergence ratio for various peak-to-valley acceleration variations assuming secular (t^2) distortion.

Depending on the type of target implosion being considered, this figure could be used to estimate the acceleration (drive) nonuniformity that a pellet could tolerate. (For example, for the implosion considered here, an acceleration uniformity of $<3\%$ peak to valley is required to avoid fuel-core distortions $>50\%$.) How this value of drive (acceleration) uniformity relates to illumination uniformity is more complicated and depends on the modeling of the processes associated

with thermal transport and energy deposition.[20,21] The acceleration nonuniformity will be caused by a temperature nonuniformity at the ablation surface resulting from a temperature nonuniformity near critical due to illumination nonuniformities. One simple model for estimating the attenuation of temperature nonuniformities between critical and ablation shows that, classically, the temperature nonuniformity will attenuate as exp $(-k\Delta R_s)$, where ΔR_s represents the separation distance between the critical and ablation surfaces and k is the wave number of the temperature perturbation given by $2\pi/\lambda$ (λ being the perturbation wavelength).[20] In spherical geometry, however, it is useful to refer to nonuniformities in terms of spherical harmonic modes (ℓ). The spherical harmonic modes are not, however, simple waves. Therefore, they can not be defined in terms of a simple wavelength. For purposes of this discussion, however, the planar wave number k and the spherical harmonic number ℓ will be related by the eigenvalue of the two-dimensional (2-D) part of the Laplacian operation resulting in $k^2 = \ell(\ell + 1)/R^2$ where R is the target radius. (For $\ell >> 1$ and a position not near the pole on the sphere $\ell \simeq 2\pi R/\lambda$.) The simple expression for the temperature attenuation becomes exp $\{-[\ell(\ell + 1)]^{1/2} \Delta R_s/R\}$ in spherical geometry. By knowing $\Delta R_s/R$ (the "smoothing ratio") one can estimate the required illumination uniformity to assure a given drive uniformity. Since simulations indicate that long-wavelength modes do not change phase during the implosion, if an average value of the time-dependent quantity $\Delta R_s/R$, shown in Fig. 37.4, is used (~ 0.35), attenuations of ~ 0.42, ~ 0.30, and ~ 0.21 would result for modes $\ell = 2$, 3, and 4, respectively. Therefore, a 3% peak-to-valley drive nonuniformity requires $\leq 7\%$ peak-to-valley illumination nonuniformity.
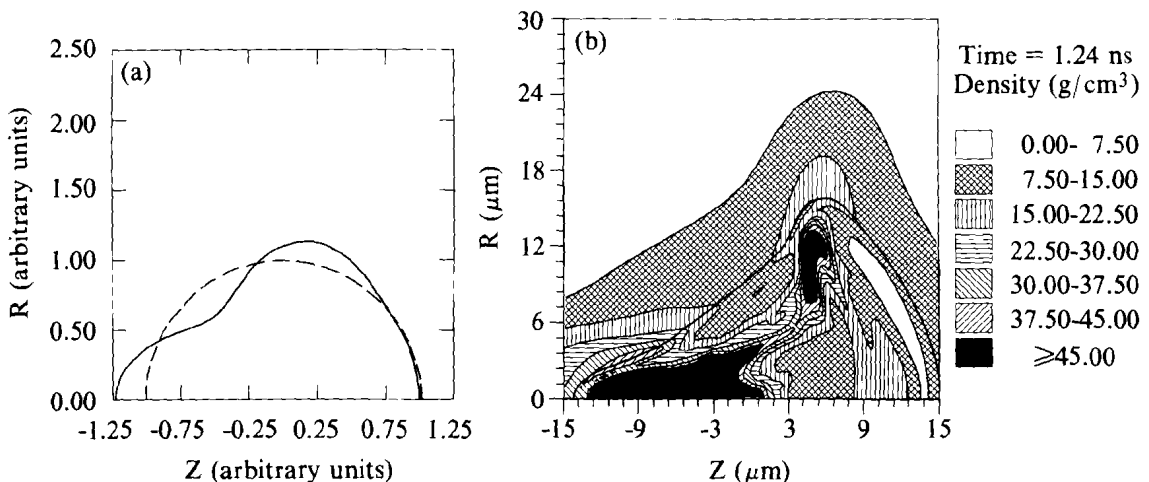

Fig. 37.4
Smoothing ratio $(\Delta R_s/R)$ and pellet-interface radii versus time for the single-shell OMEGA cryogenic implosion shown in Fig. 37.1.

TC2548

7

The above analysis, while allowing for quick estimates of the illumination uniformity required for long-wavelength modes, is potentially an over-simplification. It does not consider the full time-dependent nature of the problem, the fact that multiple-wavelength nonuniformities may be present, or the possibility of large-amplitude, long-wavelength, nonlinear, mode-mode interactions resulting in shorter-wavelength perturbations during the implosion. Moreover, the effect of long-wavelength nonuniformities on pellet performance is highly dependent on the pellet design. To give an example of the effects of long-wavelength nonuniformities on a pellet implosion, 2-D hydrodynamic simulations were performed using the program *ORCHID*. In these simulations, Legendre modes 1-4 were applied with total peak-to-valley variations of 10%-45%. (The upper end of this range is characteristic of the long-wavelength illumination nonuniformity potentially present because of power imbalance on the first high-density cryogenic implosion experiments carried out on OMEGA.) For the ~45% peak-to-valley case, Fig. 37.5(a) shows the illumination nonuniformity pattern applied for this simulation, while Fig. 37.5(b) displays the density contours at a time when the experimental yield equals the calculated yield.[22] Note that although only long-wavelength modes were initialized, their nonlinear interaction during the final stages of convergence resulted in the evolution of shorter-wavelength perturbations. When the same modes were applied with only ~10% peak-to-valley variations, the mode-mode interactions were minimized and the dominate distortions remained in the mode structure applied. The 2-D simulations have shown that another important consequence of long-wavelength perturbations is that a large fraction of the imploding materials' energy remains in the form of kinetic energy associated with large-scale motion.

Fig. 37.5
Two-dimensional *(ORCHID)* hydrodynamics simulation of implosion of pellet shown in Fig. 37.1 subjected to long-wavelength nonuniform illumination.
(a) Illumination-nonuniformity pattern placed on target (solid line) modes $1 \le \ell \le 4$, peak-to-valley of ~45%.
(b) Density contours (g/cm³) at the time when the simulation yield equaled the observed experimental yield.

TC2549

The overall effect on this type of pellet implosion is reduced DT temperatures because of the lower efficiency of kinetic-to-internal energy conversion and longer stagnation times (i.e., the final stagnation phase lasts longer than that predicted from 1-D simulations because of the large-scale mass motion of the core and ablation material during the final stagnation phase of the implosion). These 2-D simulations have shown that, for the pellet considered, the effects of long-wavelength illumination nonuniformities alone can reduce the neutron yield by a factor of ~2 in the ~10% peak-to-valley case and by a factor of ~15 in the ~45% peak-to-valley case. This does not take into account the potential effect of ablation material (SiO_2) mixing into the fuel because of shear and/or vortex-like flows that develop near the fuel-ablator interface. If these effects were included in the numerical simulations, it would be expected that the neutron yield would be reduced even further due to radiative cooling.

As stated, the effects of long-wavelength perturbations on pellet performance are highly dependent on the pellet design. The example given was a pellet implosion for which even large amounts of long-wavelength nonuniformities resulted in approximately a factor-of-10 reduction in neutron yield. However, simulations performed for high-gain direct-drive designs show that these nonuniformities must be kept below a few percent peak-to-valley to assure good pellet performance.[5] (For these designs, energy of the fuel in the form of kinetic energy associated with large-scale motion resulted in the failure of the central hot spot to ignite.) Therefore, it is very important for direct-drive fusion to be able to identify and control the sources of long-wavelength illumination nonuniformities. (As will be discussed in the next section, when long-wavelength modes coupling with short-wavelength modes is considered, the importance of the long-wavelength modes increases due to the presence of the short-wavelength perturbations.)

The next article in this edition of the LLE Review identifies a major source of long-wavelength nonuniformities for frequency-tripled glass laser systems and describes the progress that is underway to understand and control it on the OMEGA laser system. (Simulations have shown that because of the limited number and placement of individual beams on OMEGA, residual, long-wavelength nonuniformities will always be present on experiments carried out on the OMEGA laser system.)[15]

Short-Wavelength Illumination Nonuniformities

For direct-drive pellet implosions, short-wavelength nonuniformities arise mainly from individual beam profiles and their overlap on target.[15] The amplitudes and phases of these modes can change during the pellet implosions because of the motion of the critical surface and coronal plasma changes during the implosion [see Fig. 37.2(b)].[17]
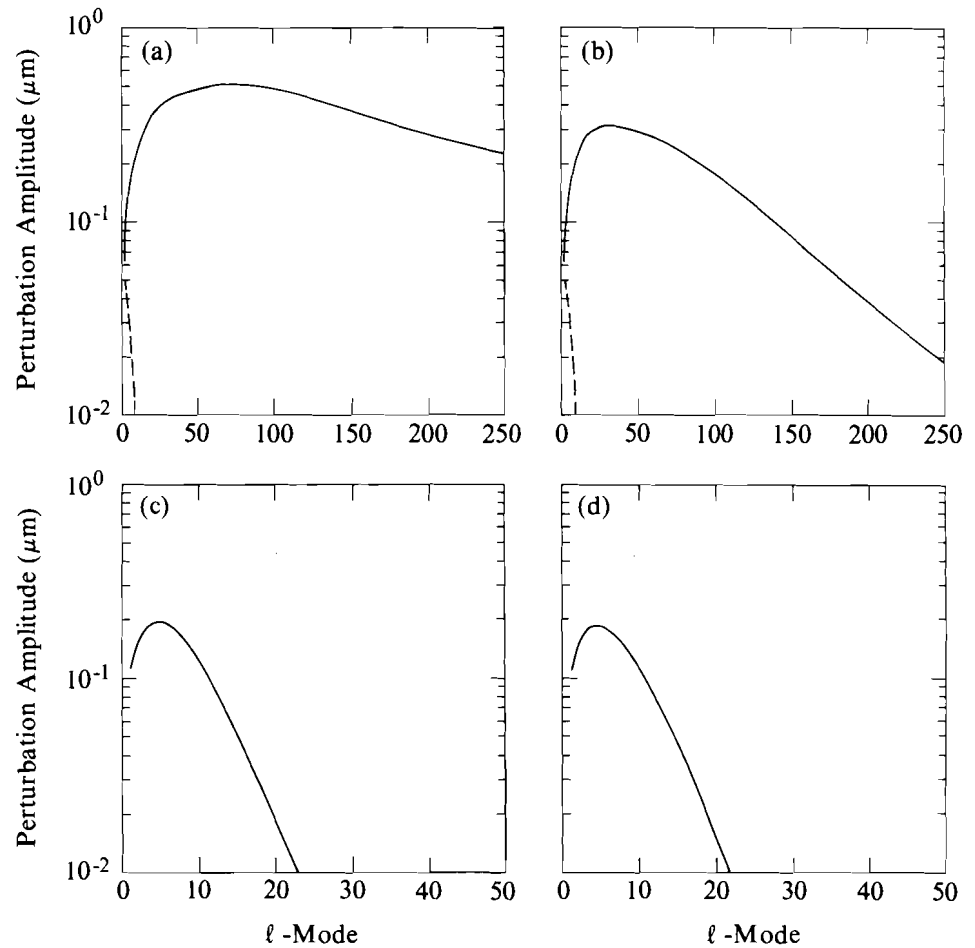
Understanding the effects of short-wavelength illumination nonuniformities on pellet performance is an area of active research for all approaches to ICF. These modes are important because they can potentially drive secular distortions, and, more importantly, act as initial amplitude "seeds" for Rayleigh-Taylor unstable growth.

Numerical simulations have shown that the ablation process affects both the linear and nonlinear growth evolution of this instability.[11-13] To estimate the importance associated with short-wavelength illumination nonuniformities, a model is required for the development of the outside-surface Rayleigh-Taylor unstable growth and its potential feed through to the inside surface of the shell. In the past, many authors have presented estimates of the consequence of Rayleigh-Taylor unstable growth on pellet performance based on a "worst-wavelength" analysis (i.e., the mode for which $\lambda_w \approx 2\pi\Delta R$, where λ_w is the "worst" mode wavelength and ΔR is a characteristic shell thickness during the implosion). Linear growth rates were obtained for this mode using perturbation methods or full 2-D simulations. Based on the growth rates obtained, the number of e-foldings expected during the implosion could be estimated. If the analysis showed that the shell could potentially rupture (the perturbation amplitude becomes comparable to the shell thickness during the implosion), then the pellet design was considered suspect. If, however, this analysis showed that the growth of this worst mode was not a problem, it was assumed that the target design was "safe" with respect to Rayleigh-Taylor unstable growth. Recently a number of important studies, both experimental[23] and theoretical,[24,25] have shown that these conclusions may have been overly optimistic. These studies now show that it is the contribution of all the unstable modes and their potential mode-mode interactions, and not just a single wavelength, that must be considered.

At this time, the treatment of all potentially unstable modes, including both linear and nonlinear evolution, during an ICF pellet implosion is beyond the capabilities of most ICF simulation programs. Therefore, models have been developed that estimate the unstable growth and its potential effect on pellet performance. These models use perturbation calculations to determine linear growth rates for the appropriate spectral range (or 2-D simulations of single-mode evolution to determine linear growth rates and nonlinear evolution information) and zeroth-order hydrodynamic information from 1-D simulations of the pellet implosion of interest. The evolution of the unstable growth development is carried out on a noninterfering (no self-consistant hydrodynamics) basis. The results can then be used to estimate the amount of shell distortion and ablator-fuel mixing that could take place during the implosion. These estimates are then used to determine the susceptibility of a given pellet design to failure due to mixing, or identify a limited region in wavelength space that is of particular importance during the implosion that can be simulated with present 2-D hydrodynamics codes. A model has been developed based on these ideas, but it treats the nonlinear saturation of unstable modes based on the interaction of a number of modes about a particular mode of interest,[25] as opposed to using results from single-mode calculations showing that a mode transits from linear to nonlinear growth when the amplitude-to-wavelength ratio becomes approximately 0.10 to 0.20.[13] A model similar to that developed in Ref. 25 will be used to obtain estimates of the importance of short-wavelength illumination nonuniformities on the cryogenic pellet implosion considered here.

Zeroth-order dynamics were obtained from the 1-D *LILAC* simulation. In this discussion, we will use the linear growth rate relation found in Ref. 11: $\gamma = \alpha \sqrt{ka} - \beta kV_a$, where $\alpha = 0.90$, $\beta \approx 3\text{-}4$, k is the wave number, a is the acceleration, and V_a is the ablation velocity that is determined from $\dot{m}/\dot{p}$ ($\dot{m}$ is the mass-flux rate and $\dot{p}$ is the peak density). This model tracks the growth of individual ℓ-modes using linear growth rates until a saturation amplitude is reached. For the outside surface instability, we are interested in the development of the bubble; therefore, once the mode goes nonlinear, the bubble grows linearly in time.[26-28] (Recent studies of finite fluid layers show that the nonlinear bubble evolution departs from this expression when the layer thickness gets small.[13,29] However, this model is used only to illustrate the potential effects of the instability; therefore, no attempt has been made to try to treat the nonlinear stages more accurately.) The model also tracks the inside-shell perturbations during the implosion. During the acceleration phase this is given by the classical feedthrough result of $\exp(-k\Delta R)$.[8] Once the inside surface begins to decelerate, this amplitude serves to seed the inside unstable growth that is evolved using the growth rate found in Ref. 14 and the density scale length of interest obtained from the *LILAC* simulation. If the mode evolves into the nonlinear region during the deceleration phase, nonlinear evolution is assumed proportional to $\delta a t^2$ in an attempt to follow the spike development, where δ is $\leq \frac{1}{2}$ ($\delta = \frac{1}{2}$ for an Atwood number equal to 1) and is obtained from 2-D simulations. There are a number of limitations associated with this kind of model; the reader is referred to Ref. 25 for a detailed discussion of these limitations and their possible consequences. (According to Ref. 25, these models can be "normalized" against the work provided by Refs. 23 and 24 as a guidance for their use at this time.)

Two model calculations are presented. The first assumes an initial amplitude of modes that is random in phase and of uniform amplitude equal to 0.01 μm for $1 \leq \ell \leq 250$. (The DPP's now in use on OMEGA have individual small-scale sizes of the order of 3 to 5 μm, and simulations of the resulting overlap pattern show that structures comparable to this size exist.)[6] This assumes that the overlap-DPP pattern imprints itself on the target uniformly. The second example assumes that some thermal smoothing of the DPP-overlap pattern has taken place before the distortions imprinted themselves on the target and was taken to be $\xi(\ell) = 0.01 \exp\{-0.01 [\ell(\ell + 1)]^{1/2}\}$, where 0.01 represents a minimal thermal smoothing ratio (see Fig. 37.4). Figures 37.6(a) and 37.6(b) show the results of these two model cases for the predicted distortions on the outside surface (solid line) and inside surface (dashed line) during the acceleration phase. It can be seen from these figures that if, as in Refs. 23 to 25, it is the amplitude of all of the unstable notes that are of importance, the reduction and/or removal of modes ≥ 25 is extremely important to pellet performance (accomplished in the second example by assuming some thermal smoothing). Figures 37.6(c) and 37.6(d) show the results for the inside unstable growth for the two cases. From these figures it can be seen that, while the assumed thermal smoothing would have an important
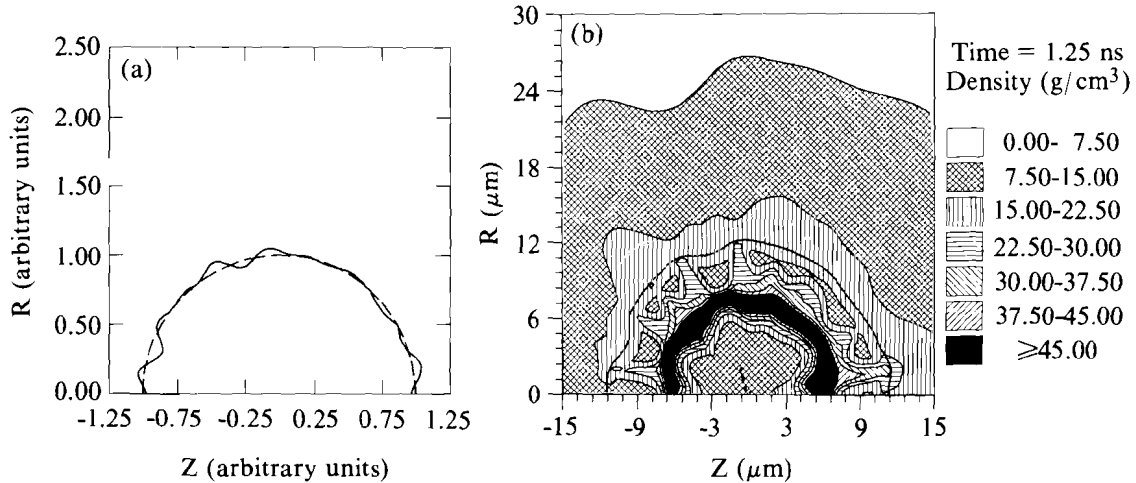
Fig. 37.6
Rayleigh-Taylor growth (model) calculations for single-shell OMEGA cryogenic pellet shown in Fig. 37.1. Two initial amplitude cases are shown. The first is for an initial amplitude of 0.01 μm for $1 < \ell < 200$. The second is for initial amplitudes given by $0.01\ e^{-0.01\ [\ell(\ell\ +\ 1)]^{1/2}}$.

(a) Ablation surface (solid line) and shell inside-surface (dashed line) growth for acceleration phase with initial amplitudes given by case 1.
(b) Same as Fig. 37.6(a) except initial amplitudes given by case 2.
(c) Inside-surface growth for case 1.
(d) Inside-surface growth for case 2.

effect on the outside unstable growth, the development of the inside instability is virtually the same for both cases.

A 2-D *ORCHID* simulation was performed to examine the behavior of this pellet when subjected to modes of nonuniformity in the range 2 through 20, which the model runs identified as important during the deceleration phase. The amplitudes of the modes were obtained from calculations of the σ_{rms} associated with the individual modes assuming perfect energy balance and the use of 24 identical DPP beams on OMEGA.[6] (The phases were randomly determined for each mode.) Both the illumination-uniformity pattern for this simulation and a density contour near the time when the simulation yield equals the experimental yield[22] are shown in Figs. 37.7(a) and 37.7(b), respectively. The large distortions in the material density in Fig. 37.7(b) are confined mainly to the inner DT-fuel region. (The glass ablator has also become distorted; however, its density variations are not apparent due to the choice of contour levels used in the figure.)

TC2551

Fig. 37.7
Two-dimensional (*ORCHID*) hydrodynamics simulation of implosion of pellet shown in Fig. 37.1 subjected to nonuniform illumination in modes $2 \le \ell \le 20$.

(a) Illumination-nonuniformity pattern placed on target (solid lines) modes $2 \le \ell \ge 20$ with a total peak-to-valley of $\sim 15\%$.

(b) Density contours (g/cm³) at the time when the simulation yield equaled the observed experimental yield.

This simulation showed that (1) the final neutron yield was reduced by approximately a factor of 10 from the 1-D simulation; (2) mixing of fuel and ablator material was confined to a region near the fuel-ablator interface; and (3) the modes were initially imprinted by the illumination-nonuniformity pattern before growing exponentially. (The Rayleigh-Taylor unstable growth is actually more complicated than the simple model examples discussed previously: Simulations show that there are actually two Rayleigh-Taylor unstable surfaces during the pellet implosion phase. The first is located at the ablation surface; the second at the DT-ablator interface where, when this interface is approximately 90 μm away from the origin, an unstable interface configuration arises with an Atwood number of ~ 0.20.) Other single-mode simulations of shorter-wavelength perturbations (ℓ = 48, 60) on this pellet have shown Rayleigh-Taylor unstable growth during the acceleration phase. However, their effect on the inside unstable development is smaller than those for $\ell \le 20$ as predicted from the simple Rayleigh-Taylor growth model. These simulations also indicate that growth is taking place over the range of modes considered to date ($\ell \le 60$). If the estimates of Rayleigh-Taylor unstable growth predicted by the simple model are correct, the treatment of all of the unstable short-wavelength modes to determine the effect on pellet performance would be required and may explain the larger departure of observed experimental yields from those which have been simulated to date. (Two-dimensional simulations are in process to more accurately determine the initial amplitude seeds potentially imposed on these implosions and their resulting linear growth rates in order to predict the potential effects of Rayleigh-Taylor unstable growth on these pellets. Once these seed amplitudes and growth rates are determined, the simple model could be used to determine if a particular region in wavelength space could be identified to examine the effect of potential fuel-ablator mixing during the implosion phase.)

The removal and/or reduction of short-wavelength illumination perturbations in direct-drive pellet implosions is extremely important. Methods to reduce these illumination modes are under study and development at a number of ICF laboratories.[30-35] At LLE, we are studying and implementing on the OMEGA laser system a method to reduce these modes—smoothing by spectral dispersion (SSD).[36] This theoretical and experimental program is presented and discussed in the third and fourth articles in this review.

In summary, we have attempted to show the potential effects of illumination nonuniformities on direct-drive pellet implosions. We have done this by breaking their effects into two relatively arbitrary categories for purposes of discussion. In reality, it is the combination of all the illumination nonuniformity modes and their potential mode-mode interactions that must be considered. (Two-dimensional simulations of the combination of large-amplitude, long-wavelength modes $\ell \leq 4$ in conjunction with short-wavelength modes $\ell \leq 20$ show that the short-wavelength modes are "carried" on the long-wavelength modes into regions in the core where they would not have been expected if only the short-wavelength modes were present.) Work is presently underway at LLE on the OMEGA laser system to address improvements over the entire range of illumination nonuniformities and experimentally investigate the effects of the residual illumination nonuniformities on direct-drive pellet implosions.

ACKNOWLEDGMENT

REFERENCES

1. J. H. Nuckolls, L. Wood, H. A. Thiessen, and G. Zimmerman, *Nature* **239**, 139 (1972).

2. J. H. Nuckolls, *Phys. Today* **35**, 24 (1982).

3. Lawrence Livermore Laboratory Laser Program Annual Report, UCRL-50021-86, 2-1 (1986).

4. R. L. McCrory, J. M. Soures, C. P. Verdon, F. J. Marshall, S. A. Letzring, S. Skupsky, T. J. Kessler, R. L. Kremens, J. P. Knauer, H. Kim, J. Delettrez, R. L. Keck, and D. K. Bradley, *Nature* **335**, 225 (1988).

5. LLE Review **23**, 125 (1985).

6. LLE Review **33**, 1 (1987).

7. J. D. Lindl (private communication).

8. G. J. Taylor, *Proc. R. Soc. London, Ser. A,* **201**, 192 (1950).

9. D. J. Lewis, *Proc R. Soc. London, Ser. A,* **202**, 81 (1950).

10. S. Chandraskhar, *Hydrodynamic and Hydromagnetic Stability* (Clarendon Press, Oxford, England, 1961), Chap. 10.

11. H. Takabe, K. Mima, L. Montierth, and R. L. Morse, *Phys. Fluids* **28**, 3676 (1985).

12. M. H. Emery, J. H. Gardner, and J. P. Boris, *Phys. Rev. Lett.* **48**, 677 (1982).

13. C. P. Verdon, R. L. McCrory, R. L. Morse, G. R. Baker, D. I. Meiron, and S. A. Orszag, *Phys. Fluids* **25**, 1653 (1982).

14. R. LeLevier, G. Lasher, and F. Bjorklund, Lawrence Livermore National Laboratory Report UCRL-4459 (1955).

15. S. Skupsky and K. Lee, *J. Appl. Phys.* **54**, 3662 (1983).

16. A. J. Schmitt and J. H. Gardner, *J. Appl. Phys.* **60**, 6 (1986).

17. P. W. McKenty, S. Skupsky, C. P. Verdon, and R. L. McCrory, *Bull. Am. Phys. Soc.* **32**, 1740 (1987).

18. W. Seka, S. D. Jacobs, J. E. Rizzo, R. Boni, and R. S. Craxton, *Opt. Commun.* **34**, 469 (1980).

19. R. S. Craxton, *Opt. Commun.* **34**, 474 (1980).

20. S. E. Bodner, *J. Fusion Energy* **1**, 221 (1981).

21. LLE Review **36**, 172 (1988).

22. LLE Review **35**, 97 (1988).

23. K. I. Read, *Physica* **12D**, 45 (1984).

24. D. L. Youngs, *Physica* **12D**, 32 (1984).

25. S. W. Haan, Lawrence Livermore National Laboratory Report, UCRL-98206 (1988).

26. G. Birkhoff and D. Carter, *J. Math. Mech.* **6**, 769 (1957).

27. P. R. Ganabedina, *Proc. R. Soc. London A* **241**, 423 (1957).

28. G. R. Baker, D. I. Meiron, and S. A. Orszag, *Phys. Fluids* **23**, 1485 (1980).

29. G. R. Baker, R. L. McCrory, C. P. Verdon, and S. A. Orszag, *J. Fluid Mech.* **178**, 161 (1987).

30. Y. Kato *et al.*, *Phys. Rev. Lett* **53**, 1057 (1984).

31. R. H. Lehmberg and S. P. Obenschain, *Opt. Commun.* **46**, 27 (1983).

32. S. P. Obenschain *et al.*, *Phys. Rev. Lett.* **56**, 2807 (1986).

33. R. H. Lehmberg, A. J. Schmitt, and S. E. Bodner, *J. Appl. Phys.* **62**, 2680 (1987).

34. R. H. Lehmberg and J. Goldhar, *Fusion Tech.* **11**, 532 (1987).

35. D. Veron *et al.*, *Opt. Commun.* **65**, 42 (1988).

36. LLE Review **36**, 158 (1988).